Hindawi
Scientific Programming
Volume 2021, Article ID 5460333, 9 pages
https://doi.org/10.1155/2021/5460333

Research Article

Extreme Learning Machine Denoising Algorithm-Based Transvaginal Three-dimensional Ultrasound Imaging on the Diagnosis Efficiency of Intrauterine Adhesions

Man He, Wan Sun, and Naxian Sha

Department of Gynecology, Ningbo No. 6 Hospital, Ningbo, 315040, China

Correspondence should be addressed to Naxian Sha; 201703226@stu.ncwu.edu.cn

Received 30 August 2021; Revised 28 November 2021; Accepted 1 December 2021; Published 23 December 2021

Academic Editor: Gustavo Ramirez

The study was intended to eliminate the noise in three-dimensional transvaginal ultrasound (3D-TVS) images and improve the diagnostic accuracy in intrauterine adhesion (IUA). The extreme learning machine (ELM) algorithm was introduced first for statement. One hundred and thirty cases of suspected IUA patients were taken as the research subjects. The denoising effects of ELM algorithm were evaluated in terms of mean square errors (MSE), peak signal-to-noise ratio (PSNR), and running time, and its diagnostic efficiency of IUA was identified from precise, specificity, and sensitivity. Furthermore, the support vector machine (SVM) algorithm was introduced for comparison. It was found that the MSE and PSNR of the ELM algorithm were 0.0021 and 64.5, respectively, and its average operation time was 11.22 ± 0.89s, that the MSE values of SVM algorithm and ELM algorithm were 0.0045 and 0.0021 and the PSNR values were 52.3 and 64.5, respectively, and that the average running time of SVM algorithm was 16.35 ± 1.33s, and the average running time of ELM algorithm was 11.22 ± 0.89s, superior to the SVM algorithm in denoising effects. Moreover, the ELM algorithm showed excellent diagnostic efficiency for patients with various degrees of IUA. In conclusion, ELM can effectively eliminate noise in 3D-TVS images and demonstrates excellent diagnostic efficiency on IUA, which is worthy of clinical application.

1. Introduction

Intrauterine adhesion (IUA) is a common gynecological disease that causes damage to the basal layer of the endometrium due to trauma or inflammation, manifested by part or complete adhesion of the cervical canal and uterine cavity [1]. Generally, the IUA patient's endometrium is damaged, leading to different degrees of fibrosis in the endometrium, which is common in pregnant women, and occurs after artificial abortion, spontaneous abortion and curettage, or postpartum hemorrhage and curettage [2, 3]. As uterine wall softens during pregnancy, it is not easy to control the curettage depth. Excessive scraping results in large negative pressure during suction, causing IUA [4]. In addition, the irregular method to dilate the cervix and repeated entry of medical devices into the uterus also increase the chance of IUA [5]. The main symptoms of IUA patients include periodic abdominal pain, dysmenorrhea, amenorrhea, and irregular menstruation. In severe cases, it may lead to female infertility. Some pregnant women with IUA may suffer from ectopic pregnancy, habitual abortion, stillbirth, etc. [6, 7], posing a huge threat to women's physical and mental health.

At present, the clinical examination methods used in IUA patients involve hysteroscopy (HSC), hysterosalpingography (HSG), sonohysterography (SHG), magnetic resonance imaging (MRI), two-dimensional transvaginal ultrasound (2D-TVS), and 3D-TVS [8, 9]. Among them, HSC examination is the gold standard for clinical diagnosis of IUA, which is able to visually inspect the internal conditions of the uterine cavity, whereas HSC is an invasive examination, and the cost of HSC examination is relatively high [10]. HSG is also an invasive examination, accompanied by many contraindications and complications.

It takes a certain period of time for women to receive HSG before they can become pregnant [11]. SHG is to inject contrast agent into uterine cavity and display uterine cavity lesions taking advantage of the good acoustic interface between the endometrium and the contrast agent. It is less traumatic, but SHG cannot clearly show the adhesion of the inspection area, suitable for simple screening [12]. MRI is a new examination method, but its application in IUA is limited. 2D-TVS examination can reflect the intrauterine conditions of IUA patients to a certain extent, but the imaging clarity is poor and the coronal section cannot be acquired. Its diagnosis accuracy of incomplete lock symptoms and mild adhesions is poor, and missed diagnosis is easy to occur [13]. 3D-TVS examination makes up for the deficiency of 2D-TVS. It can display intrauterine lesions in IUA patients, including the shape, size, and outline of the lesion. Also, it exhibits relatively good detection effects on mild adhesion. At present, 3D-TVS is extensively used for being noninvasive, simple, and less painful [14].

In clinical practice, missed diagnosis and misdiagnosis are likely to happen during 3D-TVS, which is attributed to the imaging accuracy limitation or the rotation angle limitation [15]. There is a large amount of noise in 3D-TVS images as a result of failing to process the speckles and noise in the 2D-TVS image [16]. Besides, it may cause distortion of three-dimensional images due to the actual experience and operating level limitations of clinicians, affecting the diagnosis of IUA to a certain extent.

2. Materials and Methods

2.1. Research Subjects. In this study, 138 suspected IUA patients (age range: From 23 to 48 years old; mean age: 29 ± 6.11), admitted to hospital from May 2018 to April 2020, were selected as the research subjects. The main symptoms of 138 patients were infertility, amenorrhea, and irregular menstruation. They all had a history of pregnancy and uterine cavity operation. Among them, there were 11 patients with secondary infertility (8.0%), 12 patients with amenorrhea (8.7%), 119 patients with irregular menstruation (86.2%), and 131 patients with a history of miscarriage (94.9%). All patients were diagnosed by 3D-TVS and the diagnosis results were analyzed. This study had got permission from the Medical Ethics Committee of hospital. The patients and their families had signed informed consent forms.

Inclusion criteria: (i) patients aged between 18 and 65; (ii) patients who voluntarily participated in the study and were willing to cooperate with the doctor in data collection and health surveys; (iii) patients suspected of having IUA.

Exclusion criteria: (i) patients with incomplete clinical data; (ii) patients who were unwilling to undergo HSC, 2D-TVS, and 3D-TVS examinations; (iii) patients with other serious gynecological diseases; (iv) patients who intended to be pregnant again.

2.2. The ELM Algorithm. ELM is a new and practical single-hidden layer feedforward neural network (SLGN) proposed by Professor Huang Guangbin. Compared with the traditional neural network algorithms, the ELM algorithm does not need to manually set input weights and does not need the generalized SLFN. The ELM algorithm has good generalization performance and fast learning speed and can produce the only optimal solution [17]. The implementation process of the ELM algorithm is as follows.

It is assumed that there are S different samples (a_i, d_i), where $a_i = [a_{i1}, a_{i2}, \ldots, a_{\mathrm{in}-1}, a_{\mathrm{in}}]^T \in R^n$ and $d_i = [d_{i1}, d_{i2}, \ldots, d_{\mathrm{im}-1}, d_{\mathrm{im}}]^T \in R^m$; a SLFN with C hidden layer nodes can be expressed as follows:

$$\sum_{i=1}^{C} \beta_i g_i(a_j) = \sum_{i=1}^{C} \beta_i g(\omega_i \cdot a_j + l_i), = o_j, j, = 1, 2, \ldots, N, \quad (1)$$

where C represents the hidden layer node, β represents the hidden layer output weight, g represents the activation function, ω_i represents the weight vector connecting the input data and the ith hidden layer node, β_i represents the weight vector connecting the output data and the ith hidden layer node, $\omega_i \cdot a_j$ represents the inner product of the weight vector, l_i represents the offset of the ith hidden layer point, and o_j represents the jth output sample on SLFN. The goal for an SLFN is to obtain the minimum output error value, namely,

$$\sum_{j=1}^{C} \left\| o_j - d_j \right\| = 0. \quad (2)$$

That is, there are β_i, ω_i, and l_i that satisfy the following equation:

$$\sum_{i=1}^{C} \beta_i g(\omega_i \bullet a_j + l_i) = d_j. \quad (3)$$

Equation (3) is expressed in the matrix form as follows:

$$H\beta = D, \quad (4)$$

where H represents the hidden layer output matrix of SLFN and D is the expected output matrix, and equation (5) is inferred:

$$H = [h_{ij}] = \begin{bmatrix} g(\omega_1 \cdot a_1 + l_1) & g(\omega_2 \cdot a_1 + l_2) & \ldots & g(\omega_C \cdot a_1 + l_C) \\ g(\omega_1 \cdot a_2 + l_1) & g(\omega_2 \cdot a_2 + l_2) & \ldots & g(\omega_C \cdot a_2 + l_C) \\ \vdots & \vdots & \vdots & \vdots \\ g(\omega_1 \cdot a_N + l_1) & g(\omega_2 \cdot a_N + l_2) & \ldots & g(\omega_C \cdot a_N + l_C) \end{bmatrix}_{N \times C}, \quad (5)$$

$$\beta = \begin{bmatrix} \beta_{11} & \beta_{12} & \ldots & \beta_{1m} \\ \beta_{21} & \beta_{22} & \ldots & \beta_{2m} \\ \vdots & \vdots & \vdots & \vdots \\ \beta_{C1} & \beta_{C2} & \ldots & \beta_{Cm} \end{bmatrix}_{C \times m}, \quad D = \begin{bmatrix} d_{11} & d_{12} & \ldots & d_{1m} \\ d_{21} & d_{22} & \ldots & d_{2m} \\ \vdots & \vdots & \vdots & \vdots \\ d_{N1} & d_{N2} & \ldots & d_{Nm} \end{bmatrix}_{N \times m}. \quad (6)$$

Since the ELM algorithm sets the input weight ω_i and hidden layer bias l_i of the hidden layer of the SLFN network, then the output matrix H can be uniquely determined. The training process of SLFNs can be converted to solve the $H\beta = D$ linear system, and then, the output weight β_i can be determined by 0. The least squares optimal solution of the above system is calculated as follows:

$$\widehat{\beta} = H^{\dagger}D, \tag{7}$$

where $H^{\dagger}$ represents the generalized inverse matrix of H, and then, the output sample equation of the ELM algorithm can be expressed as follows:

$$f(a) = h(a)\beta = h(a)H^{\dagger}D. \tag{8}$$

According to the orthogonal projection method, the parameter learning method of the ELM algorithm is as follows:

$$\beta = \left(\frac{\mathbf{I}}{\lambda} + H^{D}H\right)^{-1} H^{D}D. \tag{9}$$

The corresponding ELM output equation can be expressed as follows:

$$\begin{aligned} f(a) &= h(a)\beta \\ &= h(a)\left(\frac{\mathbf{I}}{\lambda} + H^{D}H\right)^{-1} H^{D}D \end{aligned} \tag{10}$$

or

$$\beta = H^{D}\left(\frac{\mathbf{I}}{\lambda} + H^{D}H\right)^{-1} D. \tag{11}$$

The corresponding ELM output equation at this time is then expressed as follows:

$$\begin{aligned} f(a) &= h(a)\beta \\ &= h(a)H^{D}\left(\frac{\mathbf{I}}{\lambda} + H^{D}H\right)^{-1} D. \end{aligned} \tag{12}$$

2.3. Denoising Process of ELM Algorithm. The ELM denoising process for three-dimensional ultrasound images is divided into two steps: training stage and testing stage. The training stage is to select the appropriate activation function and specify the number of hidden layer nodes of SLGN, and then, the algorithm starts training according to the input ultrasound image. Finally, the output weight is calculated and the image denoising model is established. The training stage is to test the noisy image according to the existing mathematical model and finally complete the denoising process [18].

It is assumed that there is an original image I_0 free of noise, and noise-added image I is obtained by adding noise to I_0. For the noisy image I, the pixel value of the local image block in I and the pixel differential derivative are extracted. For each pixel x in I, with $x(m, n)$ as the center, a partial image block $P_{m,n}$ with a size of $h \times h$ *is* obtained. The row vector $p_{(m,n)}$ is extracted with its size set as h^2. For the first-order differential and second-order differential derivative of each pixel x, the difference equation can be used to find all 5 differential values for each x. The row vector composed of all differential values is expressed as $d(m, n)$. Therefore, for each pixel x, its feature vector $u_{(m,n)}$ is extracted. The equation below is then obtained:

$$u_{(m,n)} = \left[p_{(m,n)}, d_{(m,n)}\right]. \tag{13}$$

For the original image I_0, the pixel value $I_{(m,n)}$ of I is extracted first, which is set as the target value of the extracted feature vector of the noisy image I at (m,n). Finally, the output sample $[u_{(m,n)}, I_{(m,n)}]$ of the image is obtained which is trained by the ELM algorithm to obtain the output weight of the image, followed by the establishment of a mathematical model for image denoising. Finally, the final denoising image is acquired. The ELM algorithm denoising process is shown in Figure 1.

2.4. The Parameter Setting of 3D-TVS and ELM. All patients participating in this study were diagnosed with 3D-TVS. The ultrasound diagnostic scanner was used in this study, three-dimensional volume probe 9EVF4, and the frequency of the three-dimensional volume probe was 4–8 MHz. During the transvaginal ultrasound scan, the patient took the lithotomy position. The scanning probe was covered by a condom and applied with the coupling agent. The 2D-TVS image was acquired first to display the uterine cavity morphology, intimal thickness, and sagittal section of the IUA patient, followed by the three-dimensional automatic imaging, with the scan time set to 6~8 s, the scan angle set as 130°. The 3D-TVS was carefully checked until a complete three-dimensional ultrasound image was attained. The abovementioned ultrasound examinations were performed by ultrasound specialists in obstetrics and gynecology department.

The denoising effects were mainly determined by the number of hidden layer nodes and the type of activation function [19]. Before the ultrasonic image denoising processing, the MATLAB was used to determine the parameters of the ELM algorithm. Finally, the research was carried out with the hidden layer node set as 120 and the activation function is the sigmoid function.

2.5. Accuracy Judgment Standard of IUA Diagnosis. The IUA was classified into three types: mild adhesion, moderate adhesion, and severe adhesion according to previous research results. Mild adhesions are manifested by poor endometrial growth. There are hyperechoic adhesions and discontinuous endometrium (discontinuity range <25% of the uterine cavity long diameter). Irregular small dark areas are observed, and the thickness of the endometrium is more than 5 mm. Moderate adhesions are manifested as discontinuous endometrium (discontinuity range between 25% and 75%). There are irregular hypoechoic adhesions, and the thickness of the endometrium is between 2 mm and 5 mm, and scattered separation is noted in the uterine cavity. Severe adhesions are manifested by the discontinuity of endometrium (discontinuity range >75%). The thickness of the endometrium is less

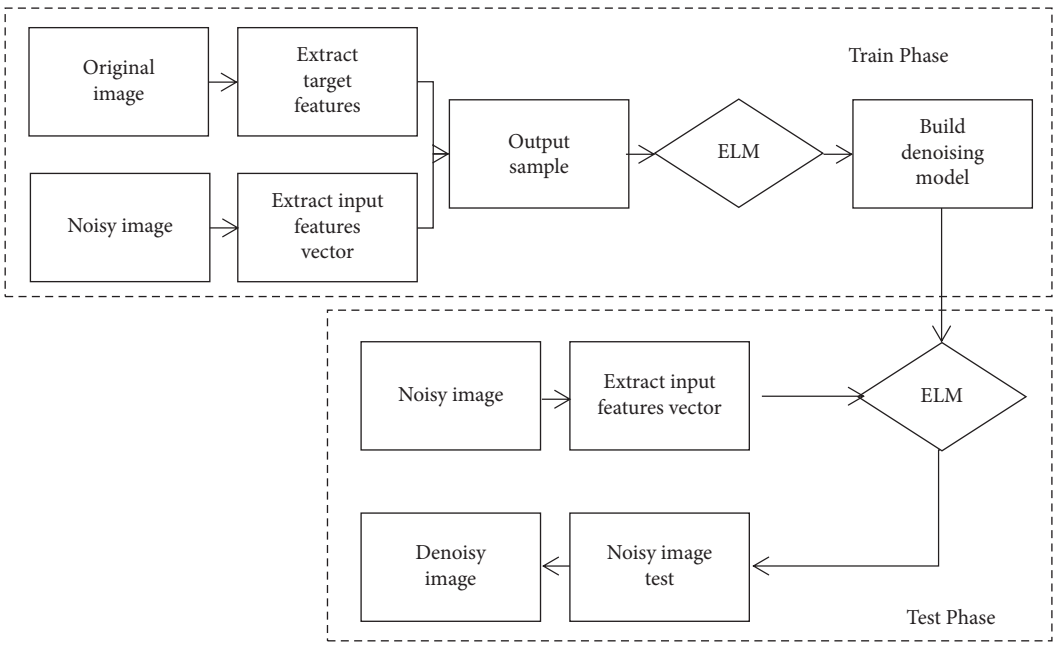

Figure 1: The schematic diagram of ELM algorithm denoising process.

than 2 mm, which cannot be distinguished from the muscle layer. There is blood in the uterine cavity, and dark areas are visible. There is no periodic change in the uterine cavity [20].

2.6. Evaluation of Diagnostic Accuracy. HSC and 3D-TVS were performed on 138 suspected IUA patients, and the HSC test results were taken as standard. The ELM was evaluated from accuracy, sensitivity, and specificity, and SVM was introduced for comparison. The calculation equations of precise, specificity, and sensitivity are as follows:

$$\begin{aligned} \mathrm{PRE} &= \frac{\mathrm{TP}+\mathrm{TN}}{\mathrm{TP}+\mathrm{TN}+\mathrm{FP}+\mathrm{FN}} \times 100\%, \\ \mathrm{SPE} &= \frac{\mathrm{TN}}{\mathrm{TN}+\mathrm{FP}} \times 100\%, \\ \mathrm{SEN} &= \frac{\mathrm{TP}}{\mathrm{TP}+\mathrm{FN}} \times 100\%, \end{aligned} \tag{14}$$

where PRE indicates accuracy, SPE indicates specificity, SEN indicates sensitivity, TP indicates number of IUA images that can be accurately identified, TN indicates that the number of nonIUA images that cannot be accurately identified, and FN indicates the number of IUA images that cannot be accurately identified.

2.7. Evaluation of Denoising Effects. The most intuitive evaluation method for 3D-TVS image quality is visual judgment, but this subjective judgment method will produce different judgment results due to the doctor's clinical experience. Consequently, MSE and PSNR were used to comprehensively judge the denoising effects of the ELM algorithm. MSE is the average error between the ideal noise-free image and the denoised image based on different denoising algorithms. A smaller MSE indicates smaller error of the denoised image. The SNR value reflects the denoising level of different algorithms. A smaller PSNR indicates smaller noise of the denoised image. The calculation methods of MSE and PSNR can be expressed as follows:

$$\begin{aligned} \mathrm{MSE} &= \frac{1}{X}\sum_{i}^{X}\left(g_i' - g_i\right)^2, \\ \mathrm{PSNR} &= 10\log_{10}\left(\frac{\sum_i^X\left(g_i - \overline{g}_i\right)}{\sum_i^X\left(g_i' - g_i\right)}\right). \end{aligned} \tag{15}$$

where X represents the number of pixels on the denoised image, g' represents the ideal image pixel gray value, g_i represents the denoised image pixel gray value, and $\overline{g}_i$ represents the average pixel value of the denoised image.

2.8. Statistics. The data was sorted out using Excel2019 and processed by SPSS17.0 software. The measurement data were calculated as $\overline{x} \pm s$. The T test was used for data conforming to the normal distribution, with the rank sum test used for data not conforming to the normal distribution. The analysis of variance was applied in multiple groups' data comparison conforming to normal distribution. $P < 0.05$ was the criterion for significance.

3. Results

3.1. Denoising Effects' Analysis. HSC and 3D-TVS examinations were performed on 138 patients suspected of having IUA, with HSC examination results used as standard, as shown in Figure 2. To test the denoising performance of the ELM algorithm, the SVM algorithm was introduced for comparison. The denoising effects are shown in Figures 3–5. The ELM was found to be superior to SVM algorithm in

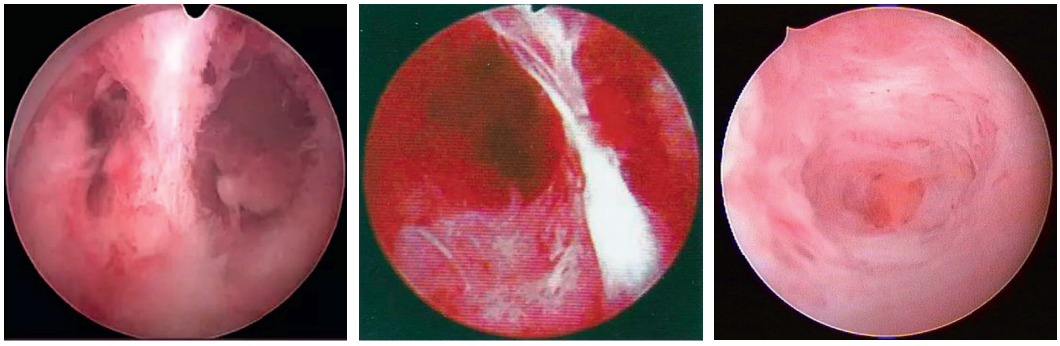

Mild Moderate Serious

Figure 2: HSC results of IUA.

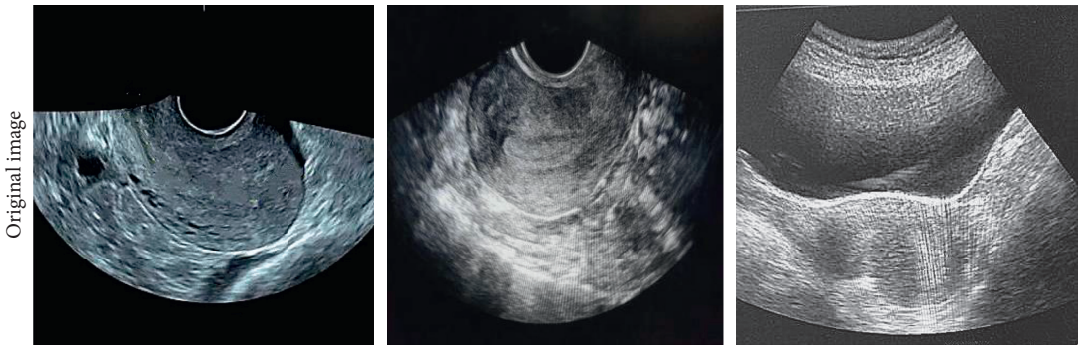

Figure 3: The original 3D-TVS images of IUA patients.

denoising effects. The ELM algorithm kept the features and structure of the image better, with clearer image edges.

To quantitatively analyze the denoising effects of different algorithms, MSE and PSNR were used as quantitative indexes. As shown in Figures 6 and 7, the ELM algorithm showed a notably lower MSE value (0.0021 vs. 0.0045) ($P < 0.05$) and a higher PSNR value (64.5 vs. 52.3) ($P < 0.05$) versus the SVM algorithm, indicating the ELM algorithm demonstrated better filtering effects. The image quality after ELM processing was higher versus the SVM.

3.2. Running Time Analysis. As shown in Figure 8, the average running time of the SVM algorithm was notably higher versus the ELM (16.35 ± 1.33 s vs. 11.22 ± 0.89 s) ($P < 0.05$), indicating that, in comparison with the SVM algorithm, ELM algorithm was more efficient in denoising.

3.3. Comparison of Diagnosis Effects. HSC examinations identified 44 patients with mild adhesions, 31 patients with moderate adhesions, and 25 patients with severe adhesions. On the basis, 3D-TVS was performed on the patients to calculate the precise, specificity, and sensitivity values of different denoising algorithms. As shown in Figure 9, when the image was processed without a denoising algorithm, the precise, specificity, and sensitivity of 3D-TVS for patients with mild adhesion were 82.3%, 81.5%, and 81.9%, respectively; those for patients with moderate adhesion were 87.7%, 84.2%, and 86.1%, respectively; those for patients with severe adhesion were 95.5%, 91.2%, and 91.4%, respectively. As shown in Figure 10, when the SVM algorithm was used to denoise the 3D-TVS image, those for patients with mild adhesions were 89.4%, 88.1%, and 90.2%, respectively; those for patients with moderate adhesions were 93.6%, 89.6%, and 91.9%, respectively; those for patients with severe adhesion were 96.2%, 92.7%, and 94.9%, respectively. As shown in Figure 11, when the ELM algorithm was used to denoise the 3D-TVS image, those for patients with mild adhesion were 96.8%, 94.4% and 92.5%, respectively; those for patients with moderate adhesion were 98.6%, 94.7%, and 94.2%, respectively; those for patients with severe adhesion were 100%, 100%, and 96.1%, respectively, showing notable differences between groups ($P < 0.05$). Hence, the ELM algorithm had higher precise, specificity, and sensitivity, demonstrating better diagnostic effects on IUA.

4. Discussion

Intrauterine birth control is a common gynecological disease, which can cause serious harm to the fertility of patients [21]. Therefore, early diagnosis is very important. 3D-TVS is used for IUA tests because it is noninvasive, simple, and painless. However, noise in 3D-TVS images will inevitably have certain influence on the accurate diagnosis of IUA [22]. In order to eliminate the noise in the 3D TV image and improve the accuracy of the image, the ELM algorithm is used to denoise the 3D TV image. One hundred and thirty eight patients with suspected intrauterine device in hospital were selected as the

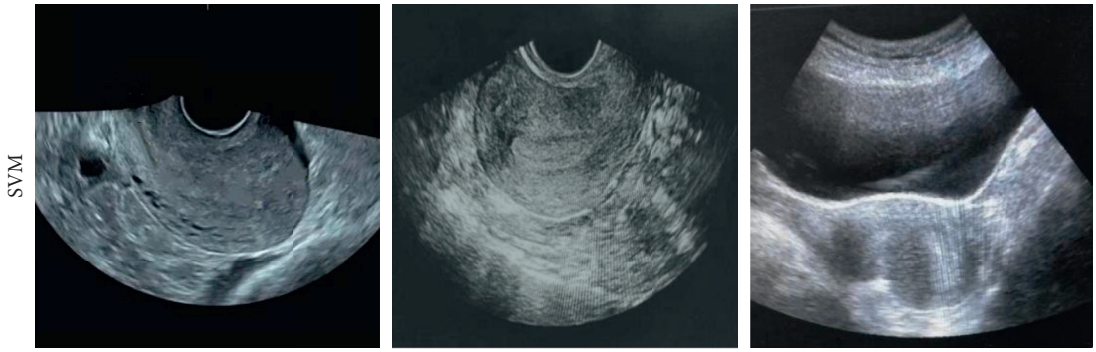

Figure 4: 3D-TVS images of IUA patients denoised by support vector machine algorithm.

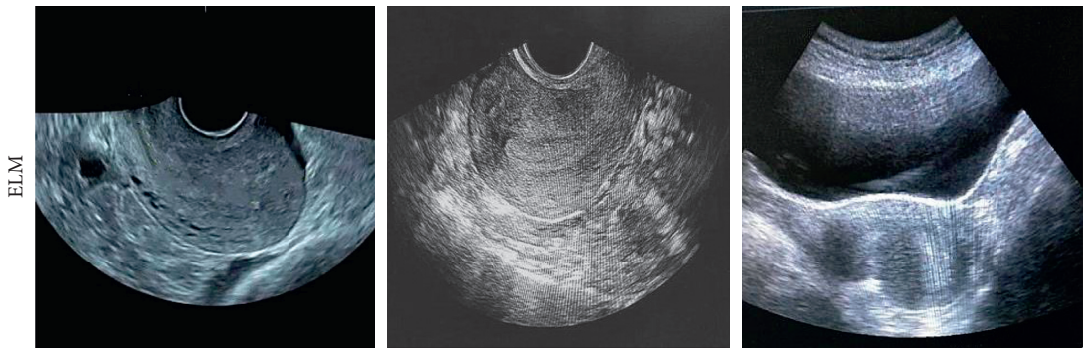

Figure 5: 3D-TVS images of IUA patients denoised by ELM algorithm.

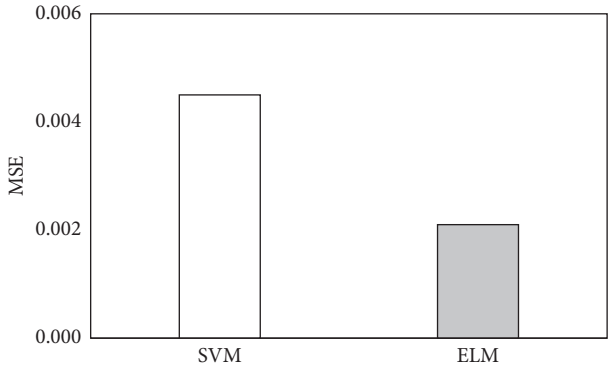

Figure 6: Comparison of MSE values.

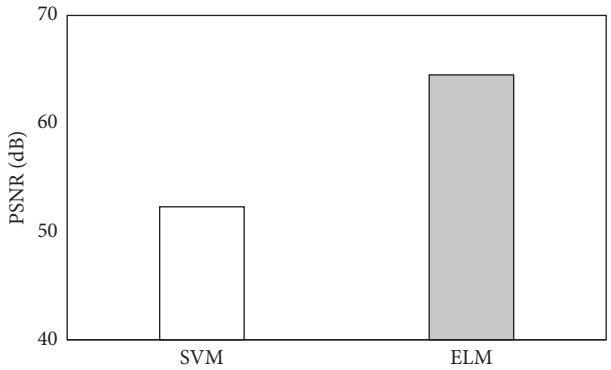

Figure 7: Comparison of PSNR values.

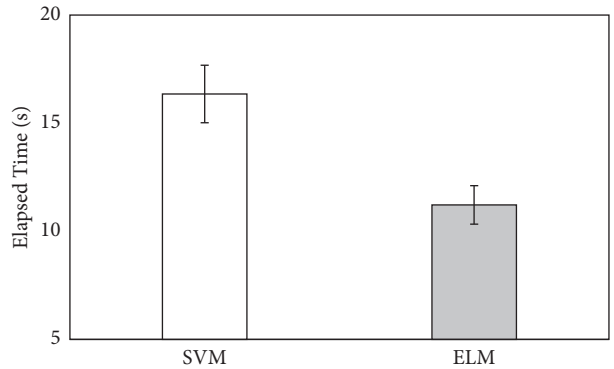

Figure 8: Comparison of running time.

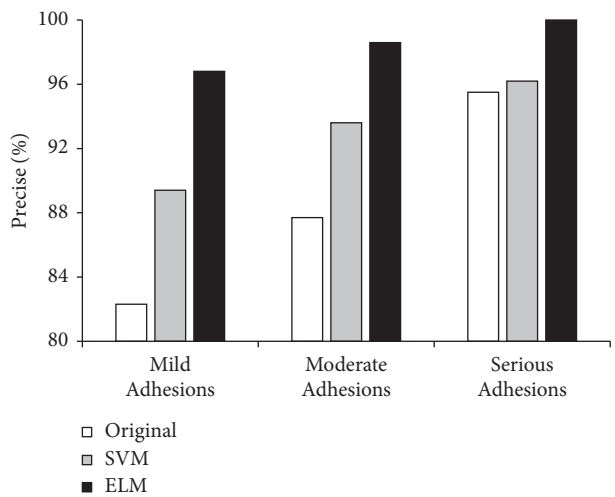

Figure 9: Comparison of precise values (annotation: original group was 3D-TVS images without denoising (the same in Figure 10)).

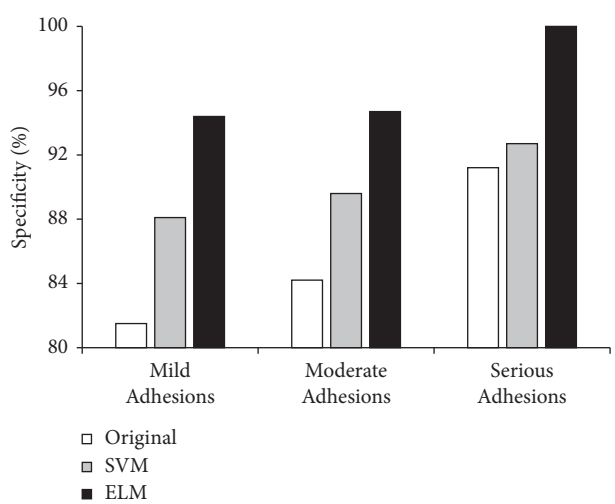

Figure 10: Comparison of specificity values.

research object. HSC and 3D-TVS were performed in 138 patients. Taking HSC diagnosis results as the gold standard, different algorithms are used to denoise 3D-TVS images. The minimum mean square error (MSE) and maximum signal-to-noise ratio (PSNR) were selected to evaluate the denoising efficiency, and the running time of the algorithm was compared to evaluate the denoising efficiency. The results showed that compared with SVM algorithm, the MSE value of ELM

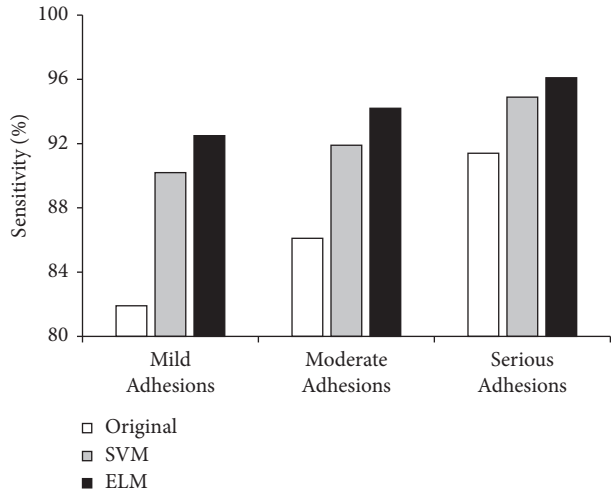

Figure 11: Comparison of sensitivity values.

algorithm decreased significantly (0.0021 vs. 0.0045) ($P < 0.05$) and the PSNR value increased significantly (64.5 vs. 52.3) ($P < 0.05$), indicating that ELM algorithm has better filtering effect. The image quality processed by ELM is better than that processed by SVM. The average running time of SVM algorithm was significantly higher than that of ELM algorithm (16.35 ± 1.33 s vs. 11.22 ± 0.89 s) ($P < 0.05$), indicating that ELM algorithm was superior to SVM algorithm in denoising. After denoising, the diagnostic effects of different algorithms on IUA were evaluated from three indexes of accuracy, specificity, and sensitivity. The results showed that the diagnosis effect of IUA patients using SVM algorithm or ELM algorithm was better than that without the denoising algorithm. However, compared with SVM algorithm, ELM algorithm has higher corresponding index, and the difference is significant ($P < 0.05$), indicating that ELM algorithm has better diagnosis effect on IUA.

5. Conclusion

In this study, the ELM algorithm was applied to the denoising of 3D-TVS images, and its denoising effects and diagnostic efficiency of the IUA were evaluated. It was found that the ELM algorithm demonstrated excellent denoising effects and high denoising efficiency on IUA patients. The ELM algorithm is suggested in 3D-TVS image denoising to improve the efficiency of IUA diagnosis. However, some limitations in the study should be noted. The sample size is small, which will reduce the power of the study. In the follow-up, an expanded sample size is necessary to strengthen the findings of the study. In conclusion, the study provides a theoretical reference for the treatment of IUA.

Data Availability

The data used to support the findings of this study are available from the corresponding author upon request.

Conflicts of Interest

The authors declare no conflicts of interest.

References

[1] L. Kou, X. Jiang, S. Xiao, Y. Z. Zhao, Q. Yao, and R. Chen, "Therapeutic options and drug delivery strategies for the prevention of intrauterine adhesions," *Journal of Controlled Release*, vol. 318, pp. 5–37, 2020.

[2] S. S Xiao, Y. J Wan, and F. J Zou, "Prevention of intrauterine adhesion with auto-crosslinked hyaluronic acid gel: a prospective, randomized, controlled clinical study," *Zhonghua Fu Chan Ke Za Zhi*, vol. 50, no. 1, pp. 32–36, 2015.

[3] Y. Q. Qi and S. M. Wang, "Research progress on the pathogenesis of intrauterine adhesions," *Medical Recapitulate*, vol. 22, no. 5, pp. 932–935, 2016.

[4] X. Liu and H. Duan, "Clinical characteristics and treatment outcome of patients with intrauterine adhesion," *Journal of Medical Research*, vol. 43, no. 8, pp. 86–89, 2014.

[5] A. B. Hooker, R. de Leeuw, and P. M. V. D. Ven, "Prevalence of intrauterine adhesions after the application of hyaluronic acid gel after dilatation and curettage in women with at least one previous curettage: short-term outcomes of a multicenter, prospective randomized controlled trial," *Fertility and Sterility*, vol. 107, no. 5, pp. 1223–1231, 2017.

[6] M. Wang, C. Liu, and B. Xia, "Advances in diagnosis and treatment of intrauterine adhesions," *Medical Information*, vol. 33, no. 8, pp. 35–339, 2020.

[7] A. Hooker, D. Fraenk, H. Brölmann, and J. Huirne, "Prevalence of intrauterine adhesions after termination of pregnancy: a systematic review," *The European Journal of Contraception and Reproductive Health Care*, vol. 21, no. 4, pp. 329–335, 2016.

[8] C. M. Chen, Y. F. Wang, and P. You, "The diagnostic value of ultrasound in intrauterine adhesions," *Journal of International Reproductive Health/Family Planning*, vol. 35, no. 2, pp. 106–108, 2016.

[9] M. K. Wang and A. M. Wang, "Diagnosis and classification of intrauterine adhesions," *Journal of Reproductive Medicine*, vol. 23, no. 4, pp. 334–338, 2014.

[10] J. Bosteels, S. V Wessel, S. Weyers et al., "Hysteroscopy for treating subfertility associated with suspected major uterine cavity abnormalities," *Cochrane Database of Systematic Reviews*, vol. 12, no. 12, Article ID CD009461, 2018.

[11] J. B. Xiong, "The diagnostic value of hysterosalpingography for intrauterine adhesion," *China Continuing Medical Education*, vol. 12, no. 8, pp. 117–119, 2020.

[12] Y. X. Gou, S. P. Zhao, and Q. M. Yang, "Effect of intrauterine acoustics combined with transvaginal three-dimensional ultrasonography on the diagnostic sensitivity and accuracy of intrauterine adhesions in patients with infertility," *Chinese Journal of Human Sexuality*, vol. 27, no. 5, pp. 71–74, 2018.

[13] F. Liu and M. R. Wang, "The value of vaginal two-dimensional ultrasonic imaging in diagnosis of intrauterine adhesions," *Journal of Medical Imaging*, vol. 26, no. 6, pp. 1138–1140, 2016.

[14] A. M. I. Mohamed, O. H. Omar, M. S. Hamed, and E. G. Dahroug, "Subendometrial blood flow changes by 3-dimensional power Doppler ultrasound after hysteroscopic lysis of severe intrauterine adhesions: preliminary study," *Journal of Minimally Invasive Gynecology*, vol. 22, no. 3, pp. 495–500, 2015.

[15] Q. Ye, E. S. Xue, and R. X. Liang, "Analysis of the diagnosis and missed diagnosis of intrauterine adhesions by three-dimensional transvaginal sonography Render and tomographic ultrasound imaging," *Chinese Journal of Ultrasonography*, vol. 29, no. 3, pp. 255–259, 2020.

[16] J. B. Lai, T. T. Lin, and D. H. Chen, "Analysis on clinical value of three-dimensional transvaginal sonography in the diagnosis of intrauterine adhesions," *Clinical Medical & Engineering*, vol. 24, no. 3, pp. 299-300, 2017.

[17] K. M. Prabusankarlal, P. Thirumoorthy, and R. Manavalan, "Classification of breast masses in ultrasound images using self-adaptive differential evolution extreme learning machine and rough set feature selection," *Journal of Medical Imaging*, vol. 4, no. 2, Article ID 024507, 2017.

[18] Y. Z. Zeng, Y. Q. Zhao, M. Liao, B. J. Zou, and X. F. Wang, "Liver vessel segmentation based on extreme learning machine," *Physica Medica*, vol. 32, no. 5, pp. 709–716, 2016.

[19] W. M. Lin, J. N. Yuan, and C. W. Feng, "Computer-aided diagnosis of alzheimer's disease based on extreme learning machine," *Chinese Journal of Biomedical Engineering*, vol. 39, no. 3, pp. 288–294, 2020.

[20] D. H. Sun, Y. L. He, and D. M. Zhang, "Predictive efficacy of different intrauterine adhesion (IUA) classification systems on the prognosis of patients with IUA," *Medical Journal of Chinese People's Liberation Army*, vol. 42, no. 5, pp. 439–444, 2017.

[21] H. Y. Chen, "Diagnostic value of two - and three - dimensional ultrasonography for intrauterine adhesions," *Radiology and Imaging*, vol. 57, no. 24, pp. 117–120, 2019.

[22] S. J. Luo, C. Li, and D. D. Tan, "Diagnostic value of three - dimensional and two - dimensional ultrasonography for intrauterine adhesions," *Radiology and Imaging*, vol. 58, no. 18, pp. 121–123, 2020.